Frontiers of Information Technology & Electronic Engineering
www.jzus.zju.edu.cn; engineering.cae.cn; www.springerlink.com
ISSN 2095-9184 (print); ISSN 2095-9230 (online)
E-mail: jzus@zju.edu.cn

Correspondence:

MIMO handset antenna for 5G/WLAN applications*

Yong CHENG†‡, Jing LU, Bing-qing SHENG

College of Electronic and Optical Engineering & College of Microelectronics, Nanjing University of Posts and Telecommunications, Nanjing 210023, China

†E-mail: chengy@njupt.edu.cn

Received Sept. 5, 2019; Revision accepted Dec. 31, 2019; Crosschecked Jan. 14, 2020

Abstract: We propose a dual-module multiple-input multiple-output (MIMO) antenna for portable terminals. The operating bands of the handheld terminal antenna are 5G (3.4–3.8 GHz) and WLAN (5.150–5.925 GHz). Antenna elements of 5G and WLAN are spaced to reduce coupling between antenna elements in the same module. The return loss of all antenna elements is larger than 6 dB. The isolation between all elements is larger than 14 dB. The radiation efficiency of the high-frequency antenna is greater than 50%, and the radiation efficiency of the low-frequency antenna is greater than 40%. The far-field gain of all elements is greater than 2.2 dBi.

Key words: Fifth-generation (5G); Handset antenna; Multiple-input multiple-output (MIMO) antenna; Decouple
https://doi.org/10.1631/FITEE.1900478 **CLC number:** TN828.6

1 Introduction

Compared with conventional wireless communication systems, the fifth-generation (5G) mobile communication system can provide higher channel capacities and higher data rates. The multiple-input multiple-output (MIMO) antenna technology (Huang et al., 2015; Cao et al., 2016; Boukarkar et al., 2018), as one of the core technologies of contemporary communication, can meet these requirements. To comply with the development trend of the Internet of Things (IoT) and communication technology, the design and research of MIMO antennas for handheld terminals (Chen and Wong, 2011; Wong, 2013) are very important.

In recent years, the research and development of MIMO terminal antennas have received much attention. A miniaturized meandered slot-line-based quad-band MIMO antenna system has been created (Hussain et al., 2019). The proposed antenna design operates in the 0.665–1.130, 1.415–2.005, 2.42–3.09, and 3.18–3.89 GHz frequency bands, thus covering most modern communication standards. A multiband eight-element MIMO antenna with an inverted π-shaped slot that acts as the decoupling element has been proposed for handheld devices (Subbaraj et al., 2019). The impedance bandwidths achieved are 170, 1070, 400, and 700 MHz. The isolation is larger than 20 dB in all the desired operating bands. A compact, low-profile, four-port, two-element antenna for the 5G IoT and handheld applications has been introduced to reduce mutual coupling, introducing rectangular slots on each side of the ground plane (Chattha, 2019). The minimum frequency range covered by the four ports of this antenna is from 2.7 to 3.6 GHz. A dual-function slot antenna at microwave frequencies and at the millimeter-wave band has also been developed (Ikram et al., 2019). It uses eight periodic feeders with a wide bandwidth of 23–29 GHz

‡ Corresponding author
* Project supported by the National and Local Joint Engineering Laboratory of RF Integration and Micro-Assembly Technology, China (No. KFJJ20170206), the Research Project of Nanjing University of Posts and Telecommunications, China (No. 208035), and the University of Macau, China (No. CPG2019-00024-FST)
ORCID: Yong CHENG, https://orcid.org/0000-0001-9864-7838

(5G) and a maximum realized gain of 12.5 dBi.

We propose a dual-module MIMO antenna for portable terminals. The handheld terminal antenna for 5G (3.4–3.8 GHz) and WLAN (5.150–5.925 GHz) is proposed. The measurement results show that the return loss of all elements is larger than 6 dB. The isolation is larger than 14 dB. The measured gain of all elements is greater than 2.2 dBi. Compared with the antennas mentioned above, in the similar frequency band, this antenna has a wider range of frequency bands and a better independence, which makes the envelope coefficient in the same frequency band lower. In addition, the omnidirectional radiation characteristics on all planes are better.

2 Design of the antenna

2.1 Design of the antenna structure

The basic structure of the antenna is shown in Fig. 1. It uses FR4 as the dielectric substrate with a thickness of 0.8 mm. The size is 150 mm×80 mm×0.8 mm, and the back is copper-clad. The structure is composed of 12 antenna elements. The high-frequency element for WLAN adopts a slot antenna, including antennas 1, 3, 5, 7, 9, and 11. The low-frequency element for 5G adopts a monopole antenna, including antennas 2, 4, 6, 8, 10, and 12. To ensure the performance of the antenna, a copper-clad is dug under the 0.5-mm-wide monopole branch. There is a gap under the slot antenna as part of the radiator. The width of the branch is 0.7 mm. Antennas 1 and 2 are spaced 29 mm apart, antennas 3 and 4 are 25 mm apart, and antennas 3 and 5 operate in the same band with a spacing of 38.8 mm. The feeding points of all 12 element are directly connected to 50-Ohm subminiature version A (SMA) connectors via the ground plane. In Fig. 1c, a 3 mm×18 mm clearance area is dug on the back plane for antenna 2 to radiate completely. Otherwise, the radiation patch is too close to the ground to meet performance standards. The length of the gap in this model is one quarter of the equivalent wavelength.

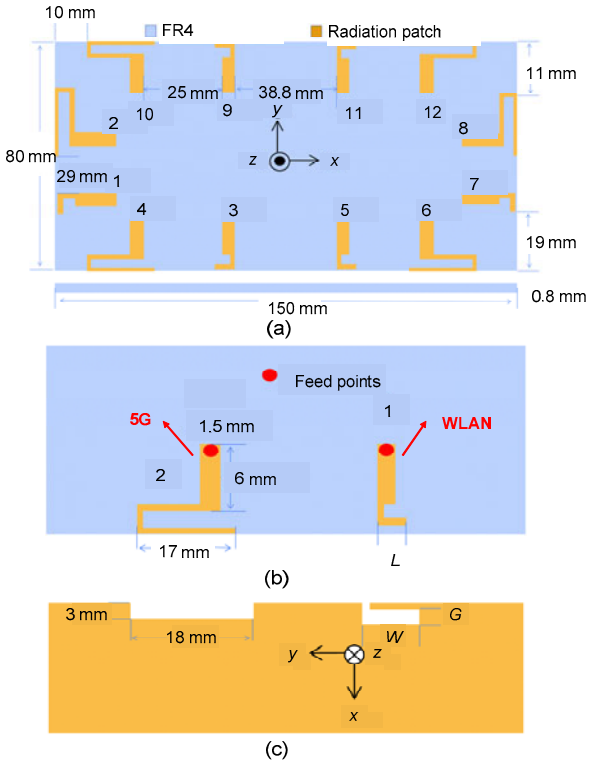

Fig. 1 Structure of the antenna: (a) top view of the antenna; (b) structure of antennas 1 and 2; (c) ground of antennas 1 and 2

2.2 Parameter analysis of the antenna

We study mainly the effect of parameters such as L (the length of radiation part), W (the length of slot), and G (the width of slot) in Figs. 1b and 1c. Fig. 2a shows the reflection of antenna 1. It can be seen that when L changes between 2.9 and 3.9 mm, the operating frequency drops from 5.6 to 5.25 GHz and the matching state worsens, meaning that the length of the branch extending from the feeding point affects not only the operating frequency, but also the matching state.

Fig. 2b shows the isolation of antennas 1 and 3, indicating that the isolation is larger than 20 dB. The change of L will not affect the isolation too much. Although the matching state is optimal at L=3.9 mm, L=3.4 mm is more suitable for balancing the operating frequency and matching.

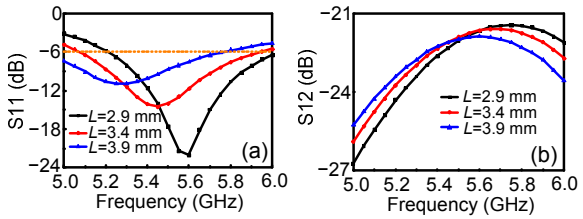

Fig. 2 Effect of L on antenna 1: (a) return loss of antenna 1; (b) isolation of antennas 1 and 3

Fig. 3 shows the results of W. Contrary to L, in Fig. 3a, when W changes from 6.2 to 7.2 mm, the operating frequency shifts to a higher one, and the return loss becomes lower, meaning that the matching also worsens as the length increases. The operating frequency is related to the current path. As W increases, some current radiates from the side of the slot, so that the current lines decrease and the operating frequency increases. Fig. 3b still shows the isolation, indicating that it can meet the requirements. W is chosen to be 6.7 mm.

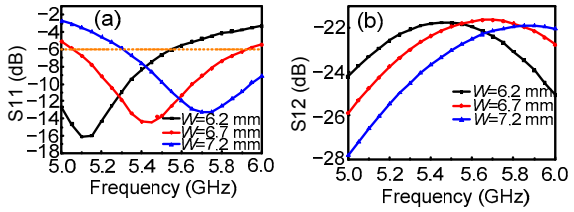

Fig. 3 Effect of W on antenna 1: (a) return loss of antenna 1; (b) isolation of antennas 1 and 3

Fig. 4a shows that when G varies between 1.8 and 2.2 mm, the return loss becomes higher and the operating frequency shifts to a higher one. It indicates that the operating frequency will get larger as the slot becomes larger, because the equivalent capacitance between the parallel metals becomes smaller. The matching between the antenna and transmission line deteriorates as the size increases. As a result, the slot is set to 6.7 mm×2 mm.

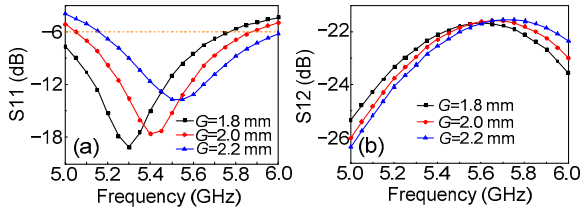

Fig. 4 Effect of G on antenna 1: (a) return loss of antenna 1; (b) isolation of antennas 1 and 3

2.3 Simulation of the antenna

According to the parameters obtained in Section 2.2, the antenna on the long side of the dielectric substrate and that on the short side are mirror-symmetrical with the opposite sides. Fig. 5 shows the S-parameters of antennas 1 and 3, and Fig. 6 shows the S-parameters of antennas 2 and 4. We choose 6 dB as the standard scribe line of the return loss, corresponding to an isolation of 10 dB. It is enough to meet the requirements. It can be seen that all S-parameters can meet the performance standards, indicating that each antenna is well matched, and that the coupling between any two of the same frequency bands is low.

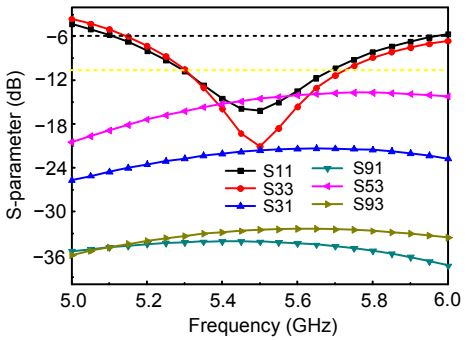

Fig. 5 S-parameters of antennas 1 and 3

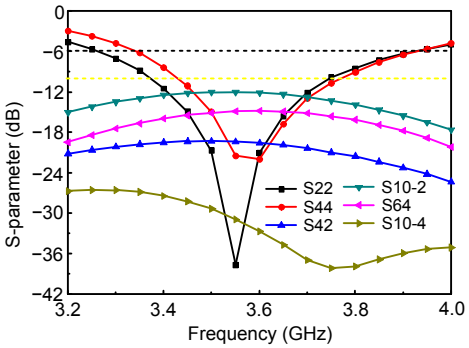

Fig. 6 S-parameters of antennas 2 and 4

Fig. 7 shows the current distribution of antennas 1 and 3 at 5.5 GHz and that of antennas 2 and 4 at 3.6 GHz. When antenna 1 is inspired, there is no significant coupling current on the adjacent antenna 9 in the high frequency. There is a weak coupling current on antenna 3, but S31 is still below −10 dB, indicating that antennas 1 and 3 will not affect each other. Similarly, antennas 3 and 5 will not affect each other. When antenna 2 is inspired, there is a coupling current on the surrounding low-frequency antennas 4 and 10, and similarly on antennas 4 and 6.

Figs. 8a and 8b show the radiation efficiencies of antennas 1 and 3, and antennas 2 and 4, respectively. It can be seen that the radiation efficiency of antennas varies from 60% to 80% within the bandwidth from low to high frequencies. This demonstrates that each antenna can radiate most of the electromagnetic waves required to complete signal transmission.

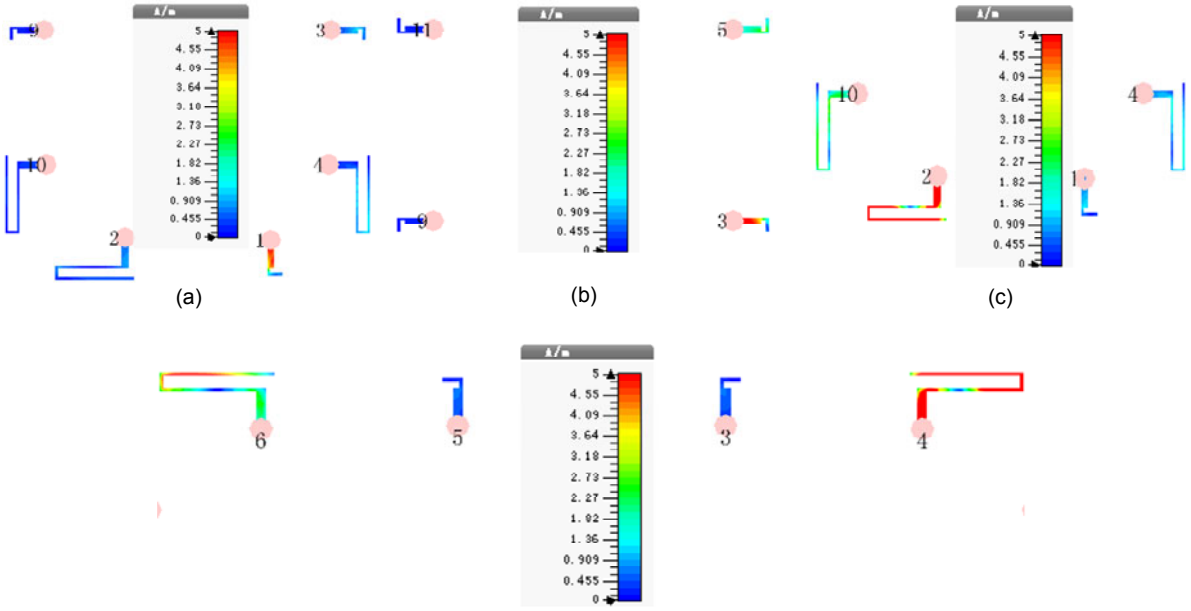

Fig. 7 Current distribution of each antenna: (a) antenna 1 at 5.5 GHz; (b) antenna 3 at 5.5 GHz; (c) antenna 2 at 3.6 GHz; (d) antenna 4 at 3.6 GHz

In addition, the envelope correlation coefficient can reflect the coupling and independence between MIMO antenna elements and reflect the diversity performance better. Fig. 9 shows the simulated envelope correlation coefficient. It can be seen that the envelope correlation coefficient of antennas 2 and 4 at the low frequency is higher than that of antennas 1 and 3 at the high frequency. The highest value is about 0.15, which is consistent with the previous discussion. The envelope correlation coefficient of all antennas is below 0.15, satisfying the index in the mobile phone MIMO multi-antenna system. The diversity performance of the antenna is good.

2.4 Experimental results and discussion

The proposed antenna has been fabricated and tested. Fig. 10a shows the top view of the antenna, and Fig. 10b is the back view of the antenna. Since the antenna is strictly mirror-symmetrical, only the S-parameters of antennas 1 and 2 and the S-parameters of antennas 3 and 4 are tested. The odd-numbered antennas are high-frequency (5.150–5.925 GHz) elements for WLAN, and the even-numbered antennas are low-frequency (3.4–3.8 GHz) elements for 5G. Fig. 10b shows the back view of antennas 1 and 2, with the left side corresponding to the clearance area below the monopole antenna 2 and the right side being the radiation slot below the slot antenna 1.

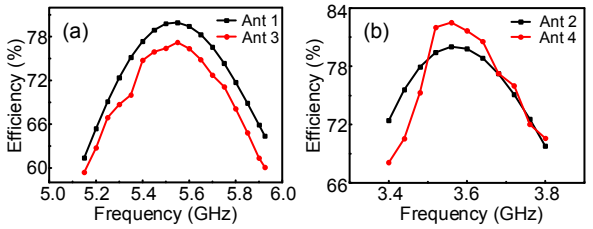

Fig. 8 Radiation efficiency of each antenna: (a) antennas 1 and 3; (b) antennas 2 and 4

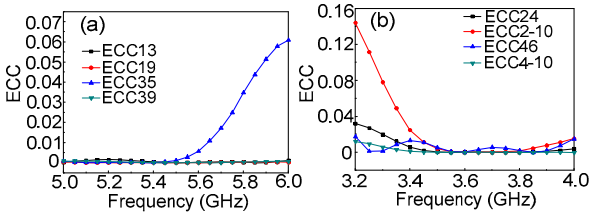

Fig. 9 Envelope correlation coefficient of antennas: (a) antennas 1 and 3; (b) antennas 2 and 4
ECC: envelop correlation coefficient

As seen in Fig. 10a, antennas at high and low frequencies are still staggered to ensure the coupling between antennas at the same frequency. Antennas are more easily coupled in the low frequency due to the larger wavelengths, so we adopt the layout form of the low, high, high, and low antenna to ensure that the adjacent low-frequency antennas are far apart.

Antennas 2 and 10 are placed vertically by orthogonal polarization so that even if they are close to each other, one will not affect the other's radiation. The isolation of antennas 2 and 10 and that of antennas 8 and 12 are both larger than 10 dB.

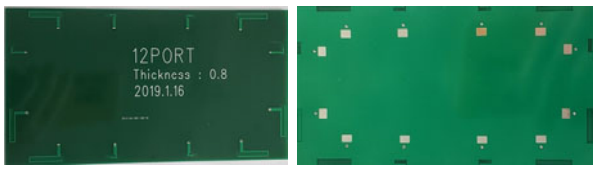

Fig. 10 Dual-module MIMO antenna: (a) top view of the antenna; (b) back view of the antenna

The measured S-parameters of antennas 1 and 3 and of antennas 2 and 4 are shown in Figs. 11a and 11b, respectively. As seen from Fig. 11a, the return loss of antenna 1 in 5–6 GHz is larger than 6 dB. Antenna 3 can cover the 5.1–6.0 GHz frequency band, which meets the requirements of 5G MIMO systems. The isolation of antennas in high-frequency bands is larger than 10 dB. In Fig. 11b, with −6 dB as the standard, antenna 2 can cover 3.20–3.95 GHz, and antenna 4 can cover 3.40–3.85 GHz, which can meet the required standard. Compared with the simulation results, the measured operating bandwidth of antennas 1 and 3 has been expanded, and the matching state is consistent with the simulation results. The isolation between antennas 3 and 5 is almost 20 dB, which has been improved. The measured bandwidth of antenna 2 is also larger than the simulation result, but the matching state of antennas 2 and 4 is not as ideal as in the simulation. This is mainly due to mismatch caused by mistakes, such as welding and machining. The measured isolation has been improved as well. The measurement results show that the S-parameters of the system meet the requirement of the indicators.

Figs. 12 and 13 show the efficiency and gain of antennas 1–4. In Fig. 12, the radiation efficiencies of antennas 1 and 3 are above 50% in the operating frequency band. The radiation efficiencies of antennas 2 and 4 are above 40% and can even reach 70%. Compared with the simulation results, the efficiency of the high-frequency antenna decreases by 8%, and the efficiency of the low-frequency antenna drops even more. This is mainly due to mismatch caused by mistakes, such as welding and machining, and the instability of the dielectric substrate. The environment of the anechoic chamber also affects the measurement results. However, it still meets the requirements in practical applications.

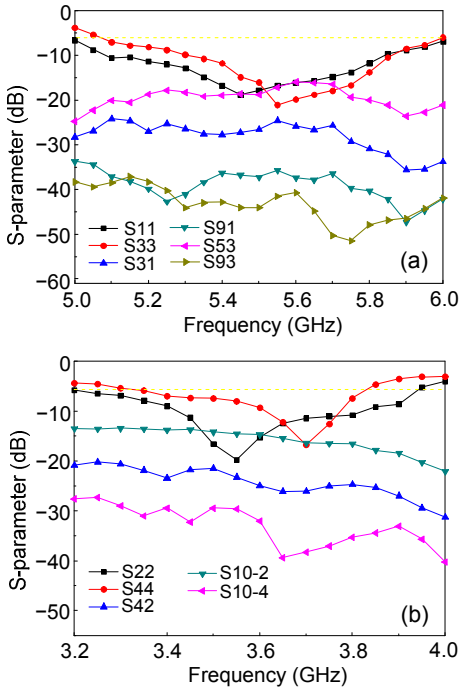

Fig. 11 Measured S-parameters: (a) antennas 1 and 3; (b) antennas 2 and 4

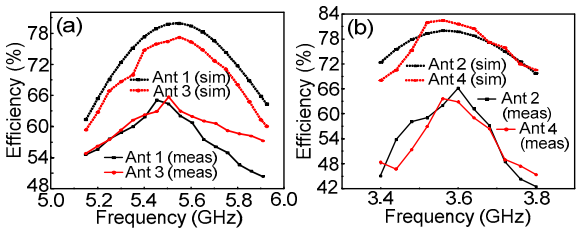

Fig. 12 Simulated and measured radiation efficiency: (a) antennas 1 and 3; (b) antennas 2 and 4

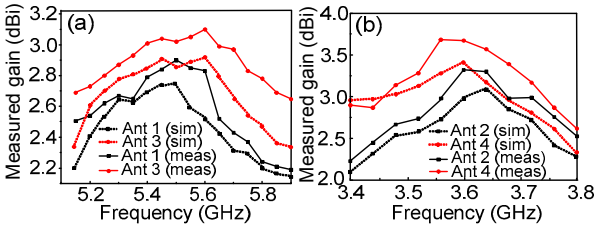

Fig. 13 Simulated and measured gain: (a) antennas 1 and 3; (b) antennas 2 and 4

Figs. 13a and 13b show the simulated and measured gains of antennas 1 and 3 and of antennas 2

and 4, respectively. The gain of antennas 1 and 3 varies between 2.2 and 3.1 dBi. The gain of antennas 2 and 4 varies between 2.25 and 3.75 dBi. Compared with the simulated gain, there is an increase of about 0.2 dBi. Comparing Fig. 12 with Fig. 13, it can be seen that the trends of the antenna efficiency and gain are consistent.

The 2D pattern of the system has been measured. As can be seen from Figs. 14a and 14b, antennas 1 and 3 have good omnidirectionality on the *xoz* and *yoz* planes. The pattern of antenna 2 is similar to that of antenna 4, with good omnidirectional radiation characteristics on all planes.

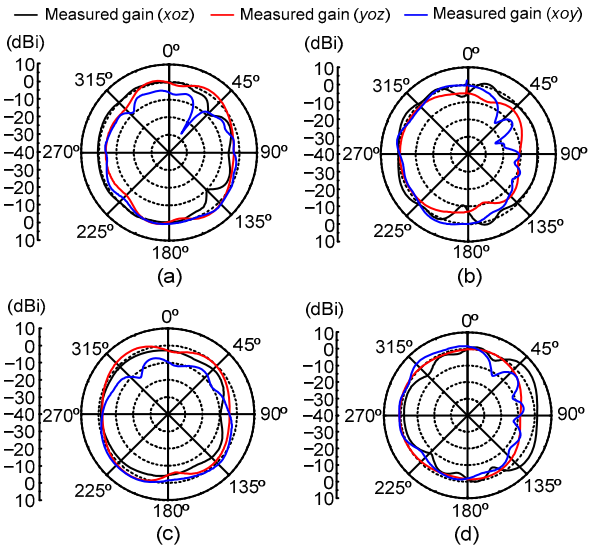

Fig. 14 Measured radiation pattern: (a) antenna 1 at 5.5 GHz; (b) antenna 3 at 5.5 GHz; (c) antenna 2 at 3.6 GHz; (d) antenna 4 at 3.6 GHz

3 Conclusions

A dual-module MIMO antenna has been proposed for 5G/WLAN portable terminals. The monopole and slot antennas have been staggered to enhance isolation. The bandwidth is approximately 1 GHz. The measured efficiency of the low-frequency antenna is above 40%, and that of the high-frequency antenna is above 50%. The gain of antennas 1 and 3 varies between 2.2 and 3.1 dBi, and that of antennas 2 and 4 varies from 2.25 to 3.75 dBi.

Contributors

Yong CHENG designed the research. Jing LU and Bing-qing SHENG processed the data. Jing LU and Bing-qing SHENG wrote the first draft of the manuscript and organized the manuscript. Yong CHENG revised and edited the final version.

Compliance with ethics guidelines

Yong CHENG, Jing LU, and Bing-qing SHENG declare that they have no conflict of interest.

References

Boukarkar A, Lin XQ, Jiang Y, et al., 2018. A miniaturized extremely close-spaced four-element dual band MIMO antenna system with polarization and pattern diversity. *IEEE Antenn Wirel Propag Lett*, 17(1):134-137. https://doi.org/10.1109/LAWP.2017.2777839

Cao YF, Cheung SW, Yuk TI, 2016. Frequency-reconfigurable multiple-input-multiple-output monopole antenna with wide-continuous tuning range. *IET Microw Antenn Propag*, 10(12):1322-1331. https://doi.org/10.1049/iet-map.2015.0295

Chattha HT, 2019. 4-port 2-element MIMO antenna for 5G portable applications. *IEEE Access*, 7:96516-96520. https://doi.org/10.1109/ACCESS.2019.2925351

Chen SC, Wong KL, 2011. Wideband monopole antenna coupled with a chip-inductor-loaded shorted strip for LTE/WWAN mobile handset. *Microw Opt Technol Lett*, 53(6):1293-1298. https://doi.org/10.1002/mop.25977

Huang H, Liu Y, Gong SX, 2015. Four antenna MIMO system with compact radiator for mobile terminals. *Microw Opt Technol Lett*, 57(6):1281-1286. https://doi.org/10.1002/mop.29074

Hussain R, Khan MU, Sharawi MS, 2019. Meandered H-shaped slot-line quad-band frequency reconfigurable MIMO antenna. Proc 13th European Conf on Antennas and Propagation, p.1-3.

Ikram M, Abbas EA, Nguyen-Trong N, et al., 2019. Integrated frequency-reconfigurable slot antenna and connected slot antenna array for 4G and 5G mobile handsets. *IEEE Trans Antenn Propag*, 67(12):7225-7233. https://doi.org/10.1109/TAP.2019.2930119

Subbaraj S, Sambandam P, Kanagasabai M, et al., 2019. Performance enhancement and signal integrity analysis of multiband MIMO antenna for handheld electronic devices. *IET Microw Antenn Propag*, 13(5):631-641. https://doi.org/10.1049/iet-map.2018.5562

Wong KL, 2013. 4G/Multiband handheld device ground antennas. Proc Asia-Pacific Microwave Conf, p.134-136. https://doi.org/10.1109/APMC.2013.6695215